

Solvent Effects on the Electronic Transitions of *p*-Nitroaniline: A QM/EFP Study

Dmytro Kosenkov and Lyudmila V. Slipchenko\*

Department of Chemistry, Purdue University, West Lafayette, Indiana, 47907

Received: October 19, 2010

Solvatochromic shifts of the electronic states of a chromophore can be used as a measure of solute–solvent interactions. The shifts of the electronic states of a model organic chromophore, *p*-nitroaniline (pNA), embedded in solvents with different polarities (water, 1,4-dioxane, and cyclohexane) are studied using a hybrid quantum mechanics/molecular-mechanics-type technique in which the chromophore is described by the configuration interaction singles with perturbative doubles (CIS(D)) method while the solvent is treated by the effective fragment potential (EFP) method. This newly developed CIS(D)/EFP scheme includes the quantum-mechanical coupling of the Coulomb and polarization terms; however, short-range dispersion and exchange-repulsion terms of EFP are not included in the quantum Hamiltonian. The CIS(D)/EFP model is benchmarked against the more accurate equation of motion coupled cluster with singles and doubles (EOM-CCSD)/EFP method on a set of small pNA-water clusters. CIS(D)/EFP accurately predicts the red solvatochromic shift of the charge-transfer  $\pi \rightarrow \pi^*$  state of pNA in polar water. The shift is underestimated in less polar dioxane and cyclohexane probably because of the omission of the explicit quantum-mechanical treatment of the short-range terms. Different solvation of singlet and triplet states of pNA results in different probabilities of intersystem crossing (ISC) and internal conversion (IC) pathways of energy relaxation in solvents of different polarity. Computed singlet–triplet splittings in water and dioxane qualitatively explain the active ISC channel in dioxane and predict almost no conversion to the triplet manifold in water, in agreement with experimental findings.

## 1. Introduction

Organic chromophore *p*-nitroaniline (pNA) belongs to a class of “push–pull” compounds with an electron-donor amino group (NH<sub>2</sub>) and an electron acceptor nitro group (NO<sub>2</sub>) connected via the  $\pi$ -conjugated system of a phenyl ring (Figure 1a). This molecule has been a subject of extensive experimental<sup>1–8</sup> studies because of its nonlinear optical properties. It has a large first hyperpolarizability and is efficient in second-harmonic generation with possible applications in photonic devices, telecommunications, and signal processing. The simple structure of pNA and its unique optical properties make it a convenient model for theoretical studies of solvent–solute interactions and the solvation of the electronic states in different environments.<sup>9</sup>

The photoexcitation from the donor to acceptor group of pNA is accompanied by charge transfer (CT) and a significant increase in the dipole moment.<sup>7</sup> This CT excited state is sensitive to solvent environments and exhibits a red solvatochromic shift in polar or polarizable solvents.<sup>1,3</sup> Ultrafast transient absorption spectroscopy measurements suggest that the CT singlet state undergoes rapid (<0.3 ps) relaxation either to the ground state by internal conversion (IC) or to the triplet manifold by intersystem crossing (ISC) depending on the polarity of a solvent.<sup>6</sup> For example, fast relaxation via ISC has been observed in dioxane and nonpolar solvents, and the triplet–triplet absorption spectra have been measured in dioxane.<sup>6</sup> However, the ISC channel is inactive in water, and the system undergoes nonradiative internal conversion.

In the current study, a combined quantum mechanics/effective fragment potential (QM/EFP) approach is used to study the effects of solvents of different polarity on singlet and triplet electronic excited states of pNA. PNA is treated using ab initio

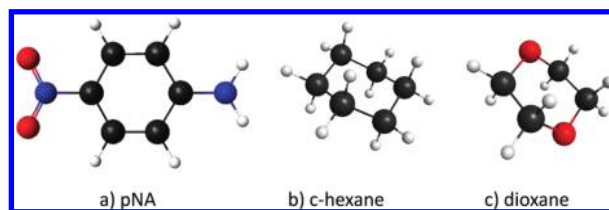


**Figure 1.** (a) Chromophore 1-amino-4-nitrobenzene or *p*-nitroaniline (pNA) and organic solvents (b) cyclohexane and (c) 1,4-dioxane.

excited-state methods (QM part), and the solvent (cyclohexane, 1,4-dioxane, or water; Figure 1), is described using the first-principles-based effective fragment potential (EFP) model potential.<sup>10,11</sup> In the EFP, each solvent molecule is represented by an effective fragment (EF) with a set of parameters determined from a preparatory ab initio calculation. The uniqueness of the EFP method is that all EFP force field parameters are derived from first principles (i.e., the method is free of parameter fitting). The EFP interaction energy is a sum of electrostatic (or Coulomb), polarization (or induction), dispersion, and exchange-repulsion terms. Through its force field, the EFP fragments can interact with each other and with ab initio components. It has been shown that EFP reproduces structures and binding energies in hydrogen- and  $\pi$ -bonded systems with an accuracy similar to or in some cases even better than that of second-order Moller–Plesset perturbation theory, MP2.<sup>12–14</sup> The EFP1 water potential was integrated with configuration interaction singles (CIS), time-dependent density functional theory (TD-DFT), and multireference perturbation theory (MRPT) methods to model the absorption spectra of chromophores in water.<sup>15,16</sup> Recently, a general EFP model was interfaced with the equation-of-motion coupled cluster with single and double excitations (EOM-CCSD) method.<sup>17</sup> The

\* Corresponding author. E-mail: lslipchenko@purdue.edu.

configuration interaction singles with perturbative doubles (CIS(D)) method<sup>18,19</sup> is a computationally more affordable alternative to EOM-CCSD.<sup>20–22</sup> A general CIS(D)/EFP interface has been developed and used in this work to describe solvatochromic shifts of the electronic states of pNA.

The structure of this article is as follows. The next section describes the theoretical details of the CIS(D)/EFP method. Section 3 provides the computational details. Benchmarks of the CIS(D)/EFP model and simulations of the absorption spectra of pNA are discussed in section 4. The conclusions are given in section 5.

## 2. Theory

There are four interaction terms in the general EFP model potential (the general EFP potential was originally called EFP2 to distinguish it from the water potential, EFP1<sup>10,23</sup>), each of which may be thought of as a truncated expansion: Coulomb (electrostatic), induction (polarization), exchange repulsion, and dispersion (van der Waals).

$$E^{\text{EFP-EFP}} = E_{\text{coul}} + E_{\text{pol}} + E_{\text{disp}} + E_{\text{exrep}} \quad (1)$$

The terms in the EFP potential may be grouped into long-range interactions, ( $1/R$ )<sup>*n*</sup> distance-dependent, and short-range interactions, which decay exponentially. The Coulomb, induction, and dispersion terms are long-range, and the exchange repulsion and damping terms are short-range. EFP has been described in detail in several papers;<sup>10,11,24–26</sup> therefore, only a brief overview of the method is presented below.

The Coulomb portion of the electrostatic interaction,  $E_{\text{coul}}$ , is obtained using the Stone distributed multipolar analysis.<sup>27,28</sup> This expansion is truncated at the octopole term. Atom centers and bond midpoints are used as expansion points. Classical Coulomb interactions become too repulsive at short range, when the electronic densities of the interacting fragments overlap and charge-penetration effects are significant. To correct for these quantum effects, electrostatic interactions are moderated by screening terms.<sup>12,29,30</sup> Overlap-based screening is used in the current study.<sup>30,31</sup>

Induction (polarization),  $E_{\text{pol}}$ , arises from the interaction of distributed induced dipoles on one fragment with a static multipole field and a field due to induced dipoles on the other fragments. The polarizability expansion is truncated at the first (dipole) term; the molecular polarizability tensor is expressed as a tensor sum of anisotropic, localized molecular orbital (LMO) polarizabilities. Therefore, the number of polarizability points is equal to the number of bonds and lone pairs in the system. The induction term is iterated to self-consistency, so it is able to capture some many-body effects.<sup>32</sup>

Dispersion interactions are expressed by an inverse  $R$  expansion:

$$E_{\text{disp}} = \sum_n C_n R^{-n} \quad (2)$$

The first term in the expansion,  $n = 6$ , corresponds to the induced dipole–induced dipole (van der Waals) interactions. In EFP, the  $C_6$  coefficient is derived from the (imaginary) frequency-dependent polarizabilities integrated over the entire frequency range.<sup>33,34</sup> Distributed dynamic polarizability tensors (centered at LMOs) are obtained using the time-dependent Hartree–Fock (HF) method. In addition, the contribution of the

$n = 8$  term is estimated to be one-third of the  $n = 6$  term. Tang–Toennies damping is used to damp the dispersion interactions at short range.<sup>35</sup>

The exchange repulsion interaction between two fragments is derived as an expansion in the intermolecular overlap, truncated at the quadratic term.<sup>36–38</sup> Kinetic and overlap one-electron integrals are calculated between each pair of fragments on the fly. Thus, each effective fragment should carry a basis set and localized wave function, with the smallest recommended basis set being 6-31++G(d,p).<sup>39</sup>

In the presence of the ab initio region, the Coulomb and polarization parts of the EFP potential contribute to the quantum Hamiltonian through additional one-electron terms:

$$\hat{H} = \hat{H}_0 + \langle p | \hat{V}^{\text{coul}} + \hat{V}^{\text{pol}} | q \rangle \quad (3)$$

The Coulomb contribution  $\hat{V}^{\text{coul}}$  to the quantum Hamiltonian consists of four terms originating from the electrostatic potential of the corresponding multipoles (charges, dipoles, quadrupoles, and octopoles). The polarization component  $\hat{V}^{\text{pol}}$  of the one-electron Hamiltonian consists of the potential due to induced dipoles of the effective fragments. Detailed expressions for the Coulomb and polarization contributions to the Hamiltonian are given in refs 10 and 26.

The induced dipoles of the effective fragments are iterated until self-consistency with each other and with the electronic wave function is achieved. The total polarization energy of the QM/EFP system (at the HF level) is

$$E_{\text{pol,gr}} = \frac{1}{2} \sum_k \sum_a^{x,y,z} [-\mu_a^k (F_a^{\text{mult},k} + F_a^{\text{nuc},k}) + \tilde{\mu}_a^k F_a^{\text{ai},k}] \quad (4)$$

where  $\mu^k$  and  $\tilde{\mu}^k$  are the induced dipole and conjugated induced dipole at the distributed polarizability point  $k$ ,  $F^{\text{mult}}$  is the field due to static fragment multipoles, and  $F^{\text{ai}}$  and  $F^{\text{nuc}}$  are the electronic and nuclear fields due to the quantum region.

In this work, dispersion and exchange-repulsion interactions between the active (ab initio) region and the effective fragments are treated similarly to the fragment–fragment interactions, as additive corrections to the total energy. As a result, the total ground-state energy of the QM/EFP system is given as

$$E_{\text{gr}}^{\text{QM/EFP}} = \langle \Phi_{\text{gr}} | \hat{H}_0 + \hat{H}^{\text{coul}} + \hat{H}_{\text{gr}}^{\text{pol}} | \Phi_{\text{gr}} \rangle + E_{\text{coul}} + E_{\text{pol,gr}} + E_{\text{disp}} + E_{\text{exrep}} \quad (5)$$

where  $\Phi_{\text{gr}}$  is the ground-state wave function,  $\hat{H}_{\text{gr}}^{\text{coul}}$  and  $\hat{H}_{\text{gr}}^{\text{pol}}$  are the Coulomb and polarization EFP contributions to the Hamiltonian, where subscript gr indicates that the induced dipoles corresponding to the electronic density of the ground state are used.  $E_{\text{coul}}$  is the electrostatic EFP–EFP energy;  $E_{\text{exrep}}$  and  $E_{\text{disp}}$  include the exchange–repulsion and dispersion energies of both EFP–EFP and ab initio–EFP regions, and  $E_{\text{pol,gr}}$  is the self-consistent ground-state polarization energy of the QM/EFP system given in eq 4.

The CIS excitation energies,  $E_{\text{CIS}}$ , are found from the eigenvalue problem

$$\begin{aligned}\hat{H}\Psi_{\text{CIS}} &= E_{\text{CIS}}\Psi_{\text{CIS}} \\ \Psi_{\text{CIS}} &= \sum_{ia} c_i^a \Phi_i^a\end{aligned}\quad (6)$$

where  $\Psi_{\text{CIS}}$  is the excited-state wave function in the subspace of all single excitations  $c_i^a$  (where  $i$  and  $a$  specify occupied and virtual orbitals, respectively).

A significant improvement to the accuracy of the CIS transition energies is achieved by introducing the perturbative correction to the energy<sup>19,40</sup>

$$E_{\text{CIS(D)}} = \langle \Psi_{\text{CIS}} | \hat{V} | U_2 \Phi_0 \rangle + \langle \Psi_{\text{CIS}} | \hat{V} | U_1 T_2 \Phi_0 \rangle \quad (7)$$

where  $\hat{V}$  is the fluctuation potential ( $\hat{V} = \hat{H} - \hat{F}$ ),  $\hat{F}$  is the mean-field Fock operator, and  $\Phi_0$  is the ground-state Hartree–Fock determinant.  $T_2$  amplitudes are from the ground-state second-order Møller–Plesset perturbation theory MP2,  $U_1$  represents the CIS amplitudes, and  $U_2$  amplitudes are found from the first-order perturbative expressions of the CIS wave function. The formal scaling of the CIS(D) model is  $N^5$ .

Each electronic state of the solute experiences the individual response of the polarizable environment such that the effective Hamiltonians of the different states differ by  $\hat{H}^{\text{pol}}$  terms. At this point, one can continue treating the polarizable environment fully self-consistently for each electronic state of interest, which results in a set of (nonorthogonal) electronic states with different effective Hamiltonians. This would correspond to method 3 described in ref 16. The orthogonality between the electronic states is necessary for the calculation of the transition properties and for the efficient gradient calculations. Although the orthogonality between subsets of the states (e.g., between the ground and excited states) can be reintroduced, the general formalism becomes more cumbersome. Additionally, the non-orthogonality of different electronic states may become an obstacle to finding several states simultaneously and would require separate Hamiltonian diagonalizations for each individual electronic state.

Alternatively, one can decouple the solute and solvent and find solutions of the CIS Hamiltonian with a constant or “frozen” response of the polarizable environment, for example, corresponding to its ground-state value. In this case, the QM/EFP excited-state energy is

$$E_{\text{ex},1}^{\text{QM/EFP}} = \langle \Psi_{\text{ex}} | \hat{H}_0 + \hat{H}^{\text{coul}} + \hat{H}_{\text{gr}}^{\text{pol}} | \Psi_{\text{ex}} \rangle + E_{\text{coul}} + E_{\text{pol,gr}} + E_{\text{disp}} + E_{\text{exrep}} \quad (8)$$

This expression corresponds to model 1 from ref 16. In particular, in case of CIS(D) eq 8 becomes

$$E_{\text{ex},1}^{\text{CIS(D)/EFP}} = \langle \Psi_{\text{CIS}} | \hat{H}_0 + \hat{H}^{\text{coul}} + \hat{H}_{\text{gr}}^{\text{pol}} | \Psi_{\text{CIS}} \rangle + E_{\text{CIS(D)}} + E_{\text{coul}} + E_{\text{pol,gr}} + E_{\text{disp}} + E_{\text{exrep}} \quad (9)$$

where the CIS wave function and the CIS(D) energy corrections were obtained with the polarization of the environment kept at its ground-state (Hartree–Fock) value.

One can include the response of the polarizable environment to the electronic density of a particular electronic state perturbatively. The one-electron density of the excited state is calculated and used to repolarize the environment (i.e., to obtain the EFP induced dipoles and polarization energy corresponding

to this state). The polarization energy  $E_{\text{pol,ex}}$  corresponding to the excited-state induced dipoles  $\mu_{\text{ex}}^k$  and  $\tilde{\mu}_{\text{ex}}^k$  is

$$E_{\text{pol,ex}} = \frac{1}{2} \sum_k \sum_a^{x,y,z} [-\mu_{\text{ex},a}^k (F_a^{\text{mult},k} + F_a^{\text{nuc},k}) + \tilde{\mu}_{\text{ex},a}^k F_{\text{ex},a}^{\text{ai},k}] \quad (10)$$

where  $F_{\text{ex}}^{\text{ai}}$  is the field due to the excited-state one-electron density. Because the polarization contribution appears in both the solute and solvent Hamiltonians (through  $\hat{H}^{\text{pol}}$  and  $E_{\text{pol}}$ , respectively), introducing the excited-state correction into the solvent part ( $E_{\text{pol,ex}}$ ) requires a counter correction in the solute part as well. This correction,  $E_{\text{pol,corr}}$ , accounts for the change in  $\hat{H}^{\text{pol}}$  upon excitation:

$$E_{\text{pol,corr}} = \langle \Psi_{\text{ex}} | \hat{H}_{\text{ex}}^{\text{pol}} - \hat{H}_{\text{gr}}^{\text{pol}} | \Psi_{\text{ex}} \rangle \cong -\frac{1}{2} \sum_k \sum_a^{x,y,z} [(\tilde{\mu}_{\text{ex},a}^k + \mu_{\text{ex},a}^k) - (\tilde{\mu}_{\text{gr},a}^k + \mu_{\text{gr},a}^k)] F_{\text{ex},a}^{\text{ai},k} \quad (11)$$

The last expression would be exact if the excited-state electronic wave function and the EFP induced dipoles were obtained self-consistently; otherwise, it is an approximation only, providing the leading contribution to the interaction of the excited-state wave function with the ground-state induced dipoles.<sup>41</sup>

By combining eqs 4, 10, and 11, we arrive at the following expression

$$\begin{aligned}\Delta E_{\text{pol}} &= \frac{1}{2} \sum_k \sum_a^{x,y,z} \\ &\left[ -(\mu_{\text{ex},a}^k - \mu_{\text{gr},a}^k) (F_a^{\text{mult},k} + F_a^{\text{nuc},k}) + (\tilde{\mu}_{\text{ex},a}^k F_{\text{ex},a}^{\text{ai},k} - \tilde{\mu}_{\text{gr},a}^k F_{\text{gr},a}^{\text{ai},k}) - \right. \\ &\quad \left. (\mu_{\text{ex},a}^k + \tilde{\mu}_{\text{ex},a}^k - \mu_{\text{gr},a}^k - \tilde{\mu}_{\text{gr},a}^k) F_{\text{ex},a}^{\text{ai},k} \right] \quad (12)\end{aligned}$$

that describes the response of the polarizable environment to the given excited state.  $\Delta E_{\text{pol}}$  is added to the electronic excitation energy of the considered state (eq 9). The first two terms in eq 12 correspond to the difference in the polarization energy of the QM/EFP system in the excited and ground electronic states. The last term is the leading correction to the interaction of the ground-state-optimized induced dipoles with the wave function of the excited state. The perturbative treatment of the response of the polarizable environment as in eqs 9 and 12 corresponds to method 2 in ref 16. This is the approach that has been implemented and used in all calculations in this article.

The developed formalism with the perturbative treatment of the polarizable environment requires a knowledge of the one-particle excited-state density. In the CIS(D) calculations, the one-particle density of the CIS wave function is used. An important advantage of the perturbative CIS(D)/EFP scheme is that the electronic wave functions of the excited states remain orthogonal to each other because they are obtained with the same (ground-state) characteristics of the polarizable environment. As mentioned above, this would not be the case if the polarization of the environment were treated fully self-consistently with the density of each electronic state. Moreover, in the perturbative scheme, any number of excited states can be found in one cycle of the iterative Davidson diagonalization procedure. This property is extensively used in this work.

TABLE 1: Singlet and Triplet Electronic Excited States of pNA in the Gas Phase<sup>a</sup>

			$E_{\text{CIS(D)}}, \text{eV}$	$E_{\text{EOM-CCSD}}, \text{eV}$	$f^b$	$\mu, \text{D}$
Singlets						
$1^1\text{A}_2$	$n \rightarrow \pi^*$	32 $\rightarrow$ 37	3.886	4.119	0.0	5.25
$1^1\text{B}_2$	$n \rightarrow \pi^*$	31 $\rightarrow$ 37	4.617	4.677	$4.22 \times 10^{-4}$	5.88
<b><math>1^1\text{A}_1</math></b>	<b><math>\pi \rightarrow \pi^*</math></b>	<b>36 <math>\rightarrow</math> 37</b>	<b>4.654</b>	<b>4.655</b>	<b><math>4.54 \times 10^{-1}</math></b>	<b>12.91</b>
$1^1\text{B}_1$	$\pi \rightarrow \pi^*$	36 $\rightarrow$ 41	4.79	4.753	$8.33 \times 10^{-3}$	9.78
$2^1\text{B}_2$	$\pi \rightarrow \text{Ryd}^c$	36 $\rightarrow$ 38	5.308	5.264	0.0	0.81
$2^1\text{B}_1$	$\pi \rightarrow \pi^*$	35 $\rightarrow$ 37	5.739	5.962	$9.26 \times 10^{-3}$	8.03
		34 $\rightarrow$ 37				
$2^1\text{A}_2$	$\pi \rightarrow \text{Ryd}^c$	36 $\rightarrow$ 39	6.216	6.127	0.0	0.99
$3^1\text{B}_1$	$\pi \rightarrow \pi^*$	34 $\rightarrow$ 37	6.219	6.447	$7.51 \times 10^{-1}$	8.60
		35 $\rightarrow$ 37				
$3^1\text{B}_2$	$\pi \rightarrow \text{Ryd}^c$	36 $\rightarrow$ 40	6.391		$1.48 \times 10^{-2}$	8.03
$2^1\text{A}_1$	$\pi \rightarrow \pi^*$	35 $\rightarrow$ 41	6.549		$3.83 \times 10^{-1}$	10.81
		36 $\rightarrow$ 44				
Triplets						
$1^3\text{A}_2$	$n \rightarrow \pi^*$	32 $\rightarrow$ 37	3.674		0.0	5.33
$1^3\text{A}_1$	$\pi \rightarrow \pi^*$	36 $\rightarrow$ 37	3.935	3.483		8.71
$1^3\text{B}_1$	$\pi \rightarrow \pi^*$	34 $\rightarrow$ 37	3.960	3.578	$7.82 \times 10^{-4}$	5.20
$1^3\text{B}_2$	$n \rightarrow \pi^*$	31 $\rightarrow$ 37	4.411	4.402	$1.00 \times 10^{-6}$	5.96
$2^3\text{B}_1$	$\pi \rightarrow \pi^*$	36 $\rightarrow$ 41	4.72	4.452	$1.04 \times 10^{-2}$	9.93
$2^3\text{A}_1$	$\pi \rightarrow \pi^*$	35 $\rightarrow$ 41	4.752	4.616	$1.27 \times 10^{-2}$	10.44
$2^3\text{B}_2$	$\pi \rightarrow \text{Ryd}^c$	36 $\rightarrow$ 38	5.183	5.114	$1.78 \times 10^{-2}$	0.68
$3^3\text{B}_1$	$\pi \rightarrow \pi^*$	35 $\rightarrow$ 37	5.276		$1.59 \times 10^{-2}$	10.49
$3^3\text{A}_1$	$\pi \rightarrow \pi^*$	36 $\rightarrow$ 44	6.153		$7.22 \times 10^{-2}$	11.95
		36 $\rightarrow$ 47				
		33 $\rightarrow$ 37				
$2^3\text{A}_2$	$\pi \rightarrow \text{Ryd}^c$	36 $\rightarrow$ 39	6.198	6.072	0.0	1.23

<sup>a</sup> EOM-CCSD/6-31+G(d) and CIS(D)/6-31+G(d) excitation energies (eV) and CIS(D)/6-31+G(d) oscillator strengths ( $f$ ) and static dipole moments ( $\mu$ , D) are shown. State assignments are done in  $C_{2v}$  symmetry. Corresponding orbitals are shown in Figure 2. <sup>b</sup> Triplet oscillator strengths are given with respect to the  $1^3\text{A}_1$  state. <sup>c</sup> Rydberg-type orbital.

### 3. Computational Details

The EFP parameters for water, cyclohexane, 1,4-dioxane, and *p*-nitroaniline (pNA) are generated using HF/6-311++G(3df,2p) in the GAMESS electronic structure package.<sup>42,43</sup> A numerical DMA procedure was used to generate distributed multipoles on pNA. EFP molecular dynamics (MD) simulations were performed in GAMESS on systems consisting of one pNA molecule and 64 solvent molecules. To account for short-range charge-penetration effects, overlap-based electrostatic screening was employed in EFP-MD simulations.<sup>30</sup> Each system was placed in a cubic box (with dimension of 12.8 Å for water, 21.0 Å for 1,4-dioxane, and 22.7 Å for cyclohexane) with periodic boundary conditions (PBC) imposed and equilibrated for 36–72 ps using a Nose-Hoover thermostat with an *NVT* ensemble at 300 K and a 1 fs time step. After equilibration, the trajectories of 30–46 ps length were prepared. To sample different solvent configurations, snapshots along these trajectories were gathered every 0.2 ps, with total of 150–230 configurations gathered. These configurations were converted into the Q-Chem input format and were used in CIS(D)/EFP calculations in the Q-Chem electronic structure package.<sup>44</sup> In all CIS(D)/EFP calculations, pNA was placed in the center of the box and treated using the CIS(D)/6-31+G(d) level of theory, and all solvent molecules were described by the EFP model potential. PBC were turned off during CIS(D)/EFP calculations.

Additionally, to assign the accuracy of CIS(D)/EFP, fully quantum CIS(D) calculations have been performed on small water–pNA clusters. The EFP water potential is identical to the one used in larger MD simulations.

Gas-phase excited states of pNA have been calculated with EOM-CCSD and CIS(D). The 6-31+G\* basis set has been employed for the quantum region in these calculations.

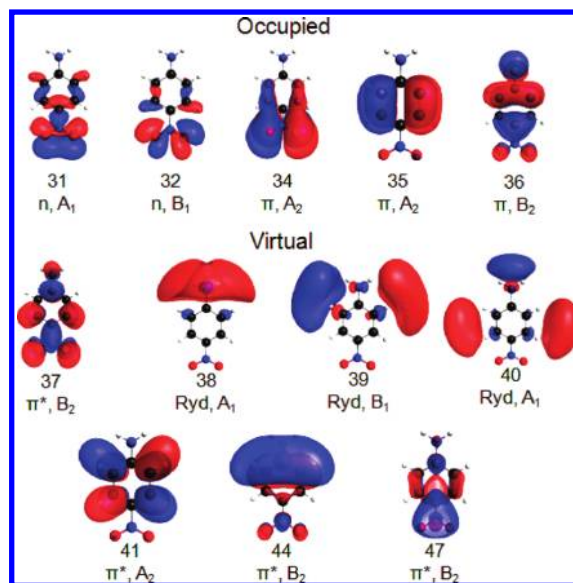


Figure 2. Molecular orbitals of pNA involved in the transitions summarized in Table 1.

### 4. Results and Discussion

**Gas-Phase Spectrum of pNA.** The low-lying electronic excited states of pNA in the gas phase calculated at the CIS(D)/6-31+G(d) and EOM-CCSD/6-31+G(d) levels of theory are summarized in Table 1. Molecular orbitals involved in these transitions are shown in Figure 2.

The lowest singlet excited state,  $1^1\text{A}_2$ , has  $n \rightarrow \pi^*$  character and zero oscillator strength. The lowest bright excitation, the  $1^1\text{A}_1$  state, corresponds to the HOMO–LUMO (36  $\rightarrow$  37)  $\pi \rightarrow \pi^*$  transition and is found to be the second or third excited state by EOM-CCSD and CIS(D). It is interesting that the CIS(D)

and EOM-CCSD excitation energies of the  $1^1A_1$  state are almost identical: 4.654 and 4.655 eV, respectively. This state has charge-transfer (CT) character (the electron density is shifted from the amino to the nitro group) and, as a result, exhibits a large dipole moment of 12.91 D. This transition has been observed in the experimental absorption spectra.<sup>1,3,6,8</sup> Several other states in the region of 6–6.5 eV have significant oscillator strengths. These states probably correspond to experimentally observed bands at 5.48 and 5.66 eV.<sup>3</sup>

Similarly to the singlets, the lowest triplet  $1^3A_2$  state has  $n \rightarrow \pi^*$  character. The oscillator strengths of the other triplets calculated with respect to this state are predominantly small ( $<5 \times 10^{-4}$ ). The exception is the  $3^3A_1 \pi \rightarrow \pi^*$  transition with an oscillator strength of  $4.91 \times 10^{-2}$  and a relatively high excitation energy of 6.153 eV. The triplet analog of the singlet CT state, the  $\pi \rightarrow \pi^*$   $1^3A_1$  transition, is the second lowest triplet excitation in the gas phase. Although the excitation in this triplet occurs between the same pair of  $\pi$  and  $\pi^*$  orbitals as in the bright CT singlet, its dipole moment of 8.7 D is significantly smaller than the dipole of the CT singlet (12.9 D). This can be explained by the covalent nature of the diradical triplet states. The diradical singlets can be either ionic or covalent in character.<sup>45</sup> Thus, even though the triplet  $1^3A_1$  state involves the excitation between spatially separated orbitals, it preserves the covalent nature and low dipole moment. As will be noted in the following discussion, different dipole moments of the formally similar singlet–triplet pair of  $A_1$  states result in different solvation and solvatochromic shifts of these states.

The oscillator strengths of the other triplets with respect to the  $1^3A_1$  state are shown in Table 1. Several states in the 4.4–5.2 eV region and  $3^3A_1$  at 6.1 eV have significant oscillator strengths  $>10^{-2}$  and could be visible in the triplet–triplet absorption spectrum.

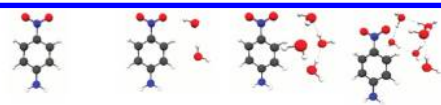
On the basis of the gas-phase results, several triplet states are energetically similar or slightly lower than the bright  $1^1A_1$  singlet state, namely,  $1^3A_2$ ,  $1^3A_1$ ,  $1^3B_1$ ,  $1^3B_2$ ,  $2^3B_1$ , and  $2^3A_1$ . In principle, all of them can contribute and enhance the probability of the intersystem crossing between the singlet and triplet manifolds. However, the relative order and energetics of these states are dramatically affected by solvents, as will be discussed in detail later on.

Generally, for the considered singlet and triplet states, there is very reasonable agreement between the CIS(D) and EOM-CCSD excitation energies. Discrepancies in the singlet-state energies do not exceed 0.25 eV, whereas larger (up to 0.45 eV) deviations are observed for some of the triplet states, particularly for the two low-lying  $1^3A_1$  and  $1^3B_1$  transitions. This is indeed surprising because, as already mentioned above, there is extremely good agreement between the CIS(D) and EOM-CCSD energies of the corresponding  $1^1A_1$  singlet state.

**Small pNA–Water Clusters.** The main goal of this section is to determine the accuracy of the CIS(D)/EFP model on the basis of several representative pNA–water clusters, for which fully quantum calculations are affordable. Additionally, the performance of CIS(D)/EFP is compared against the more accurate (and more computationally demanding) EOM-CCSD and EOM-CCSD/EFP models.<sup>17</sup>

Solvatochromic shifts in the charge-transfer  $\pi \rightarrow \pi^*$   $1^1A_1$  singlet and  $1^3A_1$  triplet states of pNA in model clusters containing two, four, and six waters are shown in Table 2. As follows from this Table, there is excellent agreement between the solvatochromic shifts calculated by CIS(D)/EFP and full CIS(D) methods; the maximum observed discrepancy is 0.03 eV. Thus, the hybrid CIS(D)/EFP method reproduces the

**TABLE 2: Gas-Phase Excitation Energies and Solvatochromic Shifts (eV) in the  $\pi \rightarrow \pi^*$   $1^1A_1$  Singlet and  $1^3A_1$  Triplet Transitions in pNA–Water Complexes**



$\pi \rightarrow \pi^*$ singlet				
Full EOM-CCSD	4.654	-0.279	-0.193	-0.263
EOM-CCSD/EFP		-0.270	-0.195	-0.239
direct polarization <sup>a</sup>		-0.008	-0.009	-0.019
Full CIS(D)	4.654	-0.336	-0.231	-0.312
CIS(D)/EFP		-0.322	-0.230	-0.280
direct polarization <sup>a</sup>		-0.004	-0.005	-0.012
$\pi \rightarrow \pi^*$ triplet				
Full EOM	3.484	-0.132	-0.087	-0.122
EOM-CCSD/EFP		-0.126	-0.088	-0.119
direct polarization <sup>a</sup>		-0.002	-0.002	-0.004
Full CIS(D)	3.934	-0.025	-0.052	0.035
CIS(D)/EFP		-0.033	-0.058	0.038
direct polarization <sup>a</sup>		0.000	0.000	-0.001

<sup>a</sup> Direct polarization contribution (i.e., “polarization correction”) to the solvatochromic shift calculated by eq 12.

excitation energies of the fully quantum CIS(D). Moreover, solvatochromic shifts by CIS(D) and CIS(D)/EFP agree reasonably well with the shifts by EOM-CCSD and EOM-CCSD/EFP, with discrepancies of  $\sim 0.05$  eV in the case of the singlet state. This result means that the electronic density of these states (which determines the response of the environment and the solvatochromic shift) is similar in CIS(D) and EOM-CCSD formulations. This behavior is indeed expected for the states with dominant single-excitation character, when CIS provides a qualitatively correct description of the wave function. In the triplet, CIS(D) is generally in worse agreement with EOM-CCSD in terms of both the gas-phase excitation energies and the solvatochromic shifts. This is probably because at the CIS(D) level the triplet  $1^3A_1$  state is strongly mixed with the energetically close  $1^3B_1$  state when the symmetry is lifted in the presence of solvent.

As discussed in ref 17, the weight of the “direct polarization” contribution (eq 12) to the solvatochromic shifts of the considered states is minor (less than 5% of the total shift). We expect that this conclusion will be true for other aqueous solutions; however, the polarization contribution may become more significant in more polar solvents or when charged species are solvated. It is not surprising that the direct polarization terms in the considered clusters are similar in the EOM-CCSD and CIS(D)-based schemes.

In general, the data in Table 2 suggest that one can approximate the excitation energy of the complex solute–solvent system by using the following energy additivity scheme:

$$E^{\text{EOM-CCSD}} \approx E^{\text{EOM-CCSD/EFP}} \approx E^{\text{CIS(D)/EFP}} + [E_{\text{gas}}^{\text{EOM-CCSD}} - E_{\text{gas}}^{\text{CIS(D)}}]$$

That is, the excitation energy of the full system by an accurate method such as EOM-CCSD may be estimated from the value of the QM/EFP energy with a simpler (computationally more affordable) QM method (e.g., CIS(D)) and the difference in the gas-phase excitation energies of the two ab initio methods.

**Solvent Polarity Effect on Solvatochromic Shifts.** Energy shifts of electronic states of a solvated chromophore depend on the polarity of the solvent. This dependence can be used as a measure of solute–solvent interactions. Excitation energies of the singlet and triplet states of pNA solvated with solvents of increasing polarity (cyclohexane, 1,4-dioxane, and water)

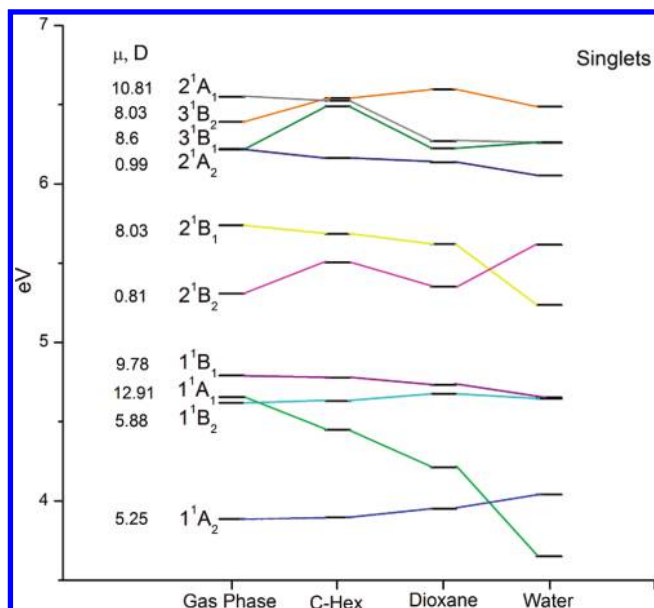


**Figure 3.** Excitation energies of the singlet electronic states of pNA in cyclohexane, 1,4-dioxane, and water compared to the gas-phase energies. Gas-phase dipole moments ( $\mu$ , D) are also shown; the ground-state dipole moment is 7.7 D. State assignments are in accordance with Table 1. The green line corresponds to the experimentally observed 1<sup>1</sup>A<sub>1</sub> CT state.

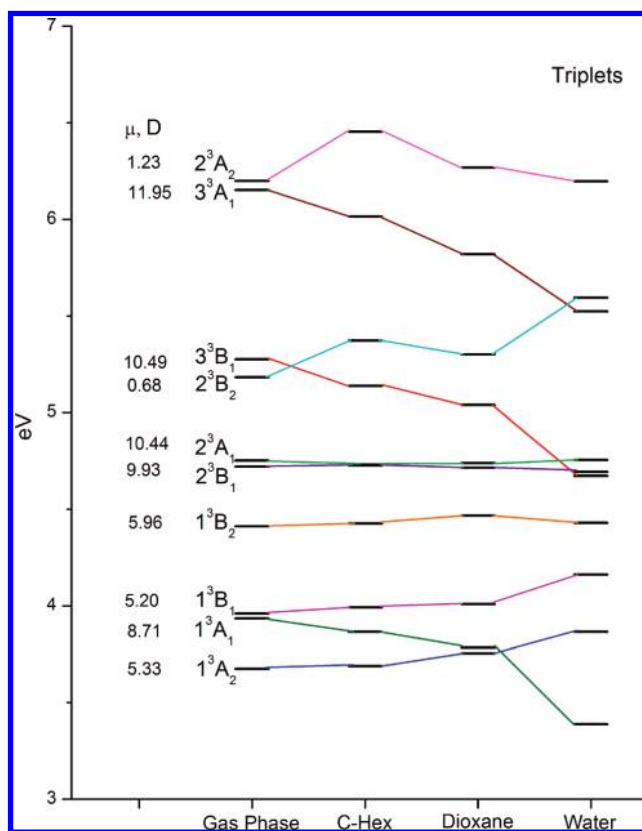


**Figure 4.** Excitation energies of the triplet electronic states of pNA in cyclohexane, 1,4-dioxane, and water compared to the gas-phase energies. Gas-phase dipole moments ( $\mu$ , D) are also shown; the ground-state dipole moment is 7.7 D. State assignments are in accordance with Table 1.

obtained from a representative MD snapshot are shown in Figures 3 and 4. For comparison, the gas-phase excitation energies and the dipole moments are also shown in these Figures. As expected, the states with larger charge separation

and larger dipole moments are stabilized by the polar or polarizable solvents and should be red-shifted. The red shift is expected to increase with increasing solvent polarity. On the contrary, the states with smaller dipole moments should be destabilized and blue-shifted in polar solvents.

As follows from Figures 3 and 4, 1<sup>1</sup>A<sub>1</sub>, 1<sup>1</sup>B<sub>1</sub>, and 2<sup>1</sup>B<sub>1</sub> singlets and 1<sup>3</sup>A<sub>1</sub>, 3<sup>3</sup>B<sub>1</sub>, and 3<sup>3</sup>A<sub>1</sub> triplets for which dipole moments are larger than the dipole of the ground state (7.7 D) demonstrate systematic red shifts upon solvation. As expected, the red shifts are larger for the states with higher dipole moments and increase in more polar solvents (in the order of cyclohexane, dioxane, and water). The largest red shift is experienced by the 1<sup>1</sup>A<sub>1</sub> charge-transfer state with a (gas-phase) dipole moment of 12.9 D. This is the state observed in experimental absorption spectra.<sup>1,3,6,8</sup>

The excitation energies of the states with smaller dipole moments than for the ground state are generally blue-shifted in polar solvents. For example, clear blue shifts are observed for the 1<sup>1</sup>A<sub>2</sub> and 2<sup>1</sup>B<sub>2</sub> singlets and the 1<sup>3</sup>A<sub>2</sub>, 1<sup>3</sup>B<sub>1</sub>, and 2<sup>3</sup>B<sub>2</sub> triplets.

The behavior of higher-lying singlets 2<sup>1</sup>A<sub>1</sub>, 2<sup>1</sup>A<sub>2</sub>, 3<sup>1</sup>B<sub>1</sub>, and 3<sup>1</sup>B<sub>2</sub> is more complicated. These states become almost degenerate in some solvents and strongly mix with each other. It should be noted that the presence of solvents lifts the symmetry constraints and allows interactions among the states belonging to different symmetries. Interactions and mixing between the states interfere with the solvent-induced shifts such that the stabilization/destabilization patterns become more complicated. A similar situation probably occurs with the 2<sup>3</sup>A<sub>2</sub> triplet state that is mixed with higher-lying excitations (not shown in Figure 4).

To summarize, as a result of interactions with a particular solvent, different electronic states experience various degrees of stabilization/destabilization and their excitation energies shift accordingly. This leads to significant changes in the excitation spectra, including the reordering of some states. For example, this is clearly seen in case of the 1<sup>1</sup>A<sub>1</sub> and 1<sup>3</sup>A<sub>1</sub> states that become the lowest singlet and triplet excitations in water but are only the second (or third) lowest excited states in less polar dioxane and cyclohexane and in the gas phase. Additionally, electronic states with solvent-modified excitation energies may experience different interaction/mixing patterns among themselves, resulting in further changes in the excitation spectra and dynamics.

Next, the absorption spectra of the 1<sup>1</sup>A<sub>1</sub> CT state in different solvents (obtained as a distribution of the excitation energy of 1<sup>1</sup>A<sub>1</sub> along the MD trajectories) were simulated. The calculated spectra, shown in Figure 5, can be unambiguously compared with the experimentally observed absorption spectra of pNA.<sup>8</sup> Obtained spectral maxima and estimated broadenings are compared with the experimental data<sup>8</sup> in Table 3.

As follows from Table 3, calculated values of spectral maxima systematically overestimate the experimentally observed values.<sup>8</sup> This can be attributed to deficiencies in the gas-phase excited-state technique (CIS(D)) and to a relatively small basis set used. However, calculated solvatochromic shifts, which are characteristic of the solvent–solute interactions and are the main target of this work, are in better agreement with the experiment. For example, both the calculated and experimentally measured red shifts in water are 1.0 eV. The calculated shifts in 1,4-dioxane and cyclohexane have errors of 0.3 and 0.2 eV, respectively. These errors could be due to a lack of short-range cavity (dispersion and exchange-repulsion) contributions to the QM/MM coupling term of the Hamiltonian that become more important in less-polar solvents. The values of the shifts as well

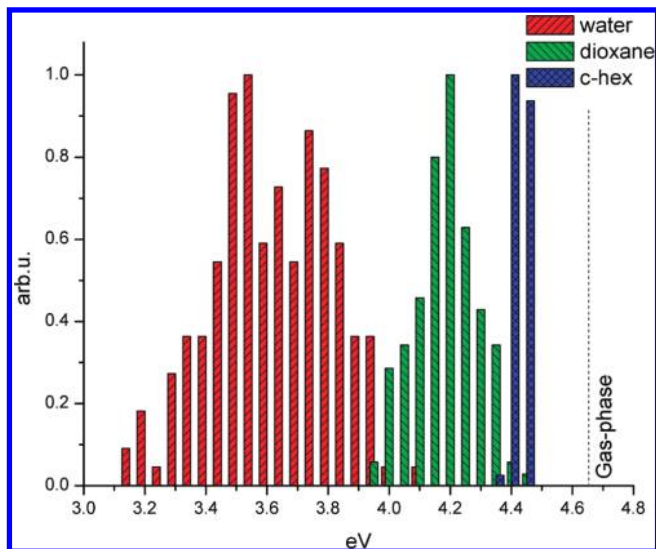


**Figure 5.** Simulated absorption spectra of the  $1^1A_1$  CT state in water (red), 1,4-dioxane (green), and cyclohexane (blue). The vertical dashed line corresponds to the energy of  $1^1A_1$  in the gas phase.

**TABLE 3: Experimental<sup>8</sup> and Calculated Positions of Spectral Maxima (Max., eV), Solvatochromic Shifts (Shift, eV), and Line Broadenings (fwhm, eV) under the Assumption of a Gaussian Line Shape**

solvent	experiment <sup>8</sup>			calculation		
	max.	shift	fwhm	max.	shift	fwhm
water	3.26	1.0	0.6	3.65	1.00	0.46
1,4-dioxane	3.54	0.72	0.6	4.21	0.44	0.24
cyclohexane	3.85	0.41	0.6	4.45	0.20	0.05
gas phase	4.26			4.65		

as the widths of the spectral lines may also be affected by keeping the geometry of the chromophore frozen and not changing it during the simulation, as was practiced in this work. For example, the frozen geometry of the chromophore may influence the spectral maximum if a particular solvent prefers (on average) a somewhat distorted geometry (e.g., with a twisted  $\text{NO}_2$  group and wagged  $\text{NH}_2$  group) that can be more or less favorable for the ground or the electronically excited state. This important issue will be investigated in detail in subsequent publications.

Additionally, the frozen geometry of the chromophore is expected to result in narrower spectral lines as a result of the omission of inhomogeneous broadening due to freezing out vibrational degrees of freedom of the chromophore. However, broadening due to different orientations of solvent molecules is still present in the simulations. However, the spectral lines become narrower in less-polar solvents. This can be explained by decreasing the solute–solvent interaction energies (polarization and Coulomb) in less-polar solvents and a smaller impact of the solvent configuration on the excitation energy. Thus, the excitation energy in nonpolar solvents is less sensitive to the different configurations of the solvent, resulting in narrower spectral lines.

**Energy Relaxation of pNA.** Experimental studies of ultrafast transient absorption dynamics of pNA<sup>6</sup> suggest that the singlet CT state undergoes either a fast internal conversion (IC) to the ground state or intersystem crossing (ISC) to the triplet manifold. Moreover, the efficiency of ISC strongly depends on the solvent and is higher in less-polar solvents. For example, the time constant of ISC in 1,4-dioxane is  $\leq 0.8$  ps but is  $\leq 10$  ps in water. In dioxane, after ISC to the triplet manifold, the triplet absorption spectrum was also recorded.<sup>6</sup>

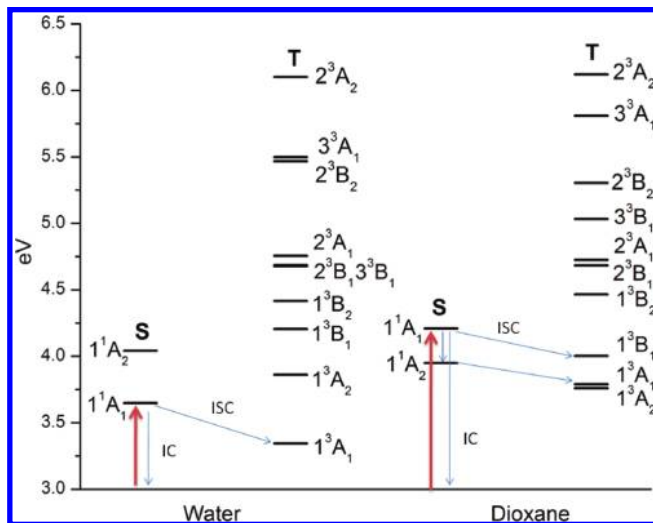


**Figure 6.** Scheme of the pNA relaxation dynamics in water and in dioxane. Red arrows correspond to the intense absorption band due to excitation to the  $1^1A_1$  CT state. This excitation further undergoes either internal conversion (IC) or intersystem crossing (ISC) to the triplet manifold (shown by blue arrows).

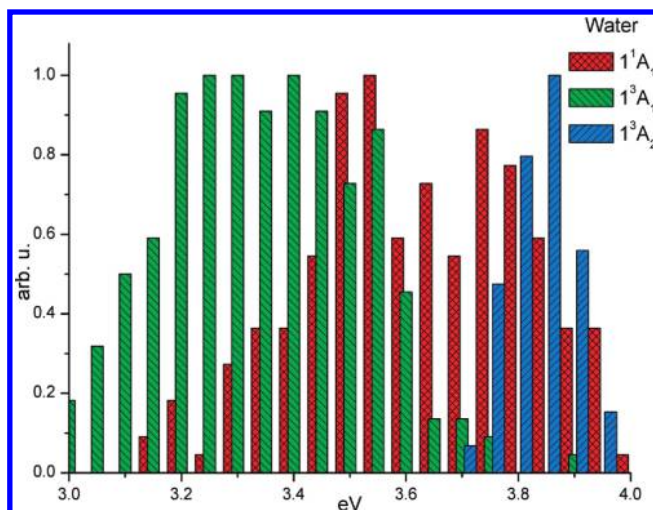


**Figure 7.** Distribution of the excitation energies of the  $1^1A_1$  singlet and the  $1^3A_1$  and  $1^3A_2$  triplets of pNA in water.

A scheme of the relaxation dynamics of pNA in water and dioxane is presented in Figure 6. Upon excitation to the  $1^1A_1$  singlet state, the energy may relax via IC and/or ISC mechanisms.

According to refs 46 and 47, the transition probability for ISC can be written as follows:

$$P_{\text{ISC}} = \left(\frac{2\pi}{\hbar}\right) \rho \langle S | \hat{H}_{\text{so}} | T \rangle^2 \sum_n \langle \phi''_n | \phi'_0 \rangle^2 \cdots \quad (13)$$

$\rho$  is the density of states,  $\hat{H}_{\text{so}}$  is the spin–orbit coupling operator,  $\phi'_0$  is the zeroth-level vibrational wave function of singlet S, and  $\phi''_n$  represents all vibrational wave functions of triplet T. To ensure a high density of states  $\rho$ , the singlet and triplet states contributing to the transition rate should have a small energy splitting. Thus, the relative rates of IC and ISC depend on the energy splitting between the initial singlet and energetically accessible triplets, and a denser manifold of the triplet states increases the probability of ISC.

To get nonvanishing matrix elements  $\langle S | \hat{H}_{\text{so}} | T \rangle$  in eq 13, the direct product of singlet and triplet wave functions  $S \times T$  should

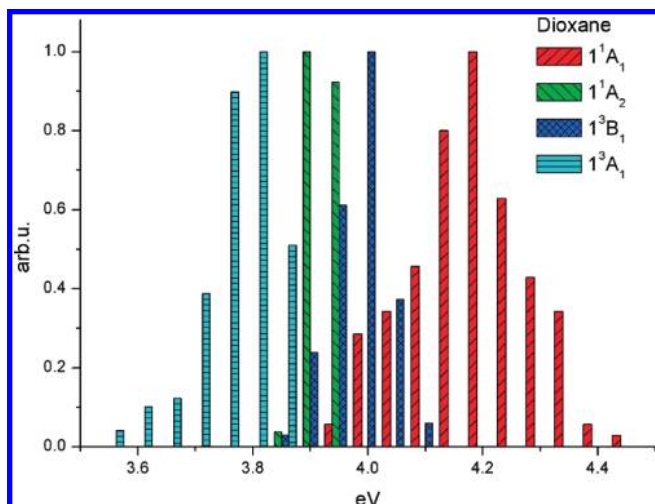


**Figure 8.** Distribution of the excitation energies of the  $1^1A_1$  and  $1^1A_2$  singlets and the  $1^3B_1$  and  $1^3A_1$  triplets of pNA in dioxane.

belong to the same irreducible representation of the molecular point group as one of the components of rotation  $R_x$ ,  $R_y$ , or  $R_z$ .<sup>46</sup> In  $C_{2v}$ , this means that the  $S \times T$  product should belong to any of the  $A_2$ ,  $B_1$ , or  $B_2$  symmetries. For example,  $1^1A_1 \rightarrow 1^3B_1$  and  $1^1A_2 \rightarrow 1^3A_1$  transitions will have nonvanishing  $\langle SH_{so}|T \rangle$  matrix elements and the  $1^1A_1 \rightarrow 1^3A_1$  or  $1^1A_2 \rightarrow 1^3A_2$  transition is forbidden (in the gas phase). Because the symmetry of the state is related to its character, one can simply say that the spin-orbit coupling and ISC rate are higher for states with different character, such as for a  $\pi \rightarrow \pi^*$  singlet and  $n \rightarrow \pi^*$  triplet pair.<sup>45–47</sup>

Additionally, to provide enough singlet–triplet mixing, the structure of vibrational levels of the singlet and triplet should fit and at least one of the electronic states should have a dense manifold of vibronic levels.

The following discussion provides a qualitative analysis of the possibility of ISC in water and dioxane on the basis of our calculations of electronic spectra of pNA in these solvents. However, one should note that a static picture (corresponding to nonequilibrium solvation) is presented here because no optimization of the excited states or state-specific relaxation of the solvent was considered. A more revealing and much more intricate investigation of ISC in pNA would involve following the dynamics of the CT state and analyzing the ST couplings along the trajectory. This task will be left for future work.

As follows from Figure 6, only one triplet state lies below  $1^1A_1$  in water. This is the triplet counterpart of  $1^1A_1$ , the  $1^3A_1$  state with  $\pi \rightarrow \pi^*$  character. El-Sayed's rules suggest that the ISC to this state will be very slow because of the vanishing  $\langle SH_{so}|T \rangle$  matrix element. The  $1^3A_2$  triplet with  $n \rightarrow \pi^*$  character, which is favorable for ISC, has (on average) higher energy than the  $1^1A_1$  singlet, which makes the probability of ISC very low.

To analyze the singlet–triplet splittings further, the excitation energies of the low-lying triplet states were sampled and compared to the energy distribution of the  $1^1A_1$  singlet. These plots, showing the overlap of the states in water and dioxane, are presented in Figures 7 and 8. Additionally, the singlet–triplet energy splittings were directly calculated and sampled along the MD trajectories, as shown in Figure 9. As follows from Figure 7, there is on average a nonzero overlap between the CT singlet and both  $1^3A_2$  and  $1^3A_1$  triplets in water.

However, the plots of the singlet–triplet splittings (Figure 9a,b) are more informative. For example, a very broad distribution of the  $1^3A_2-1^1A_1$  splitting (Figure 9a) suggests that at some solvent configurations these two states may be exactly degenerate and ISC may be possible. The distribution of the  $1^3A_1-1^1A_1$  splitting in water (Figure 9b) is much narrower, which is

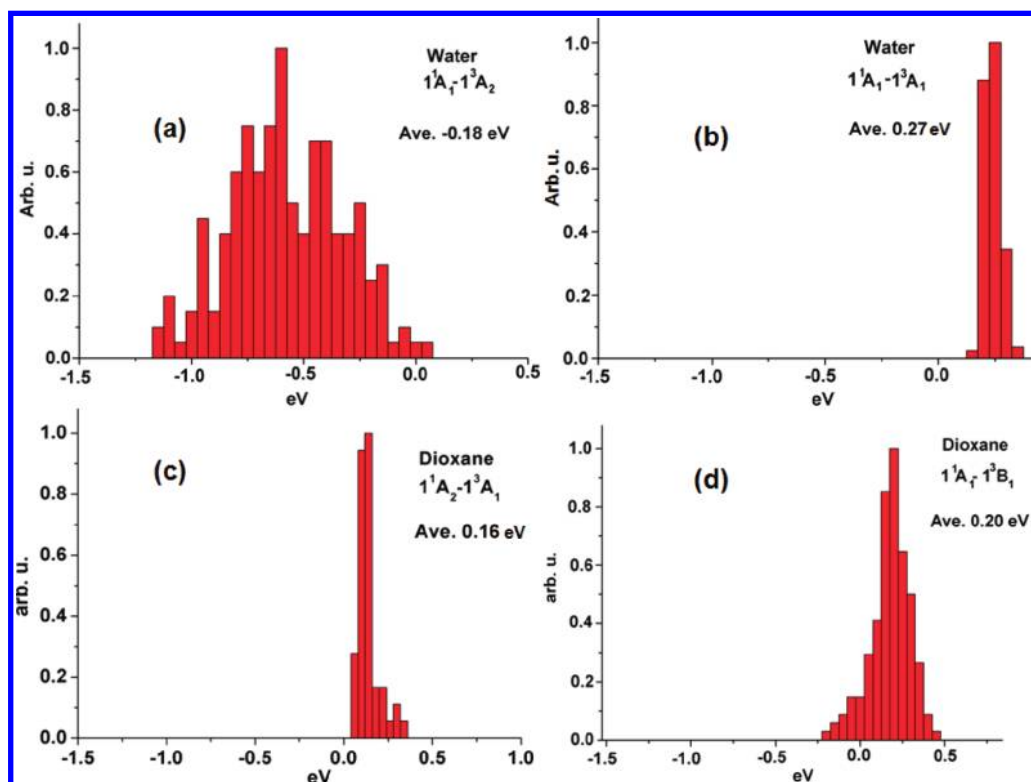


**Figure 9.** Distribution of the singlet–triplet energy splittings for (a)  $1^1A_1-1^3A_2$  and (b)  $1^1A_1-1^3A_1$  in water and (c)  $1^1A_2-1^3A_1$  and (d)  $1^1A_1-1^3B_1$  in dioxane. Average values (Ave.) of the splittings are also shown.



expected because these states have similar natures (both of them are  $\pi \rightarrow \pi^*$  diradical states) and are perturbed by the solvent in similar ways.

The ordering of the states is very different in dioxane. First, the  $1^1A_1$  state is not the lowest singlet but is preceded by the  $1^1A_2$   $n \rightarrow \pi^*$  state. Thus, an additional possible channel for energy relaxation is nonradiative decay from  $1^1A_1$  to  $1^1A_2$  and ISC from  $1^1A_2$  to either  $1^3A_1$  or  $1^3B_1$ , both of which have  $\pi \rightarrow \pi^*$  character and thus are favorable candidates for ISC. Moreover, the three triplet states ( $1^3B_1$ ,  $1^3A_1$ , and  $n \rightarrow \pi^*$   $1^3A_2$ ) lie below the CT  $1^1A_1$  singlet, also providing good opportunities for energy relaxation. The experimentally recorded triplet absorption spectrum in dioxane<sup>6</sup> suggests that the  $1^3A_1$  triplet is populated because it is the only state that shows significant oscillator strengths with respect to other triplets within the energy range of  $\sim 3$  eV (Table 1). The energy relaxation pathway consistent with the experimental observation is IC from  $1^1A_1$  to  $1^1A_2$  and ISC from  $1^1A_2$  to  $1^3A_1$ . This channel is even more favorable in less polar solvents such as cyclohexane, where the  $1^1A_2$ – $1^3A_1$  splitting decreases because of a smaller red shift of  $1^3A_1$ .

As seen in Figure 8, there is a significant overlap between  $1^1A_1$  and  $1^3B_1$  and between  $1^1A_2$  and  $1^3A_1$  in dioxane. Moreover, as follows from Figure 9c,d, the average value of the  $1^1A_2$ – $1^3A_1$  energy splitting is 0.16 eV and the average  $1^1A_1$ – $1^3B_1$  splitting is 0.2 eV and has a broader distribution. Thus, both transitions may contribute to ISC.

## 5. Conclusions

The hybrid QM/MM-type technique combining the CIS(D) method with the EFP potential is developed and used for the investigation of the solvatochromic shifts of pNA in water, dioxane, and cyclohexane. The electronic spectrum of pNA is described by CIS(D), and the solvent molecules are treated with EFP. The CIS(D)/EFP scheme employs quantum-mechanical coupling of the Coulomb and polarization terms of the quantum and EFP Hamiltonians. Benchmarks of the CIS(D)/EFP scheme on a set of small pNA–water clusters suggest that it accurately (within 0.05 eV) describes the solvatochromic shifts in polar solvents.

The CIS(D)/EFP absorption spectrum of pNA in water is in excellent agreement with experimental data, with a solvatochromic shift of 1.0 eV. The simulated spectra in dioxane and cyclohexane have discrepancies with the experimental spectra in terms of both the shifts (0.2–0.3 eV) and line widths. A possible reason for these deviations is the omission of QM/MM coupling for the short-range dispersion and exchange-repulsion terms that dominate solute–solvent interactions in nonpolar solvents. The development of exchange-repulsion and dispersion coupling terms is underway.

The relaxation mechanisms of the CT singlet excited state of pNA in water and 1,4-dioxane are considered, and the probabilities of IC and ISC are qualitatively analyzed. Different solvations of singlet and triplet states of pNA result in a denser manifold of the low-lying triplet states and smaller singlet–triplet energy splittings that facilitate ISC in dioxane. These findings are in qualitative agreement with experimental data.

**Acknowledgment.** This work was supported by an NSF Career grant (CHE-0955419), an ACS PRF grant (49271-DNI6), and Purdue University. We thank Professor Mark Gordon, Dr. Federico Zahariev, Dr. Pooja Aurora, and Sarom Sok for many fruitful discussions related to this work.

## References and Notes

- (1) Farztdinov, V. M.; Schanz, R.; Kovalenko, S. A.; Ernsting, N. P. *J. Phys. Chem. A* **2000**, *104*, 11486.
- (2) Fujisawa, T.; Terazima, M.; Kimura, Y. *J. Phys. Chem. A* **2008**, *112*, 5515.
- (3) Millefiori, S.; Favini, G.; Millefiori, A.; Grasso, D. *Spectrochim. Acta, Part A* **1977**, *33*, 21.
- (4) Moran, A. M.; Kelley, A. M. *J. Chem. Phys.* **2001**, *115*, 912.
- (5) Schuddeboom, W.; Warman, J. M.; Biemans, H. A. M.; Meijer, E. W. *J. Phys. Chem.* **1996**, *100*, 12369.
- (6) Thomsen, C. L.; Thogersen, J.; Keiding, S. R. *J. Phys. Chem. A* **1998**, *102*, 1062.
- (7) Wortmann, R.; Kramer, P.; Glania, C.; Lebus, S.; Detzer, N. *Chem. Phys.* **1993**, *173*, 99.
- (8) Kovalenko, S. A.; Schanz, R.; Farztdinov, V. M.; Hennig, H.; Ernsting, N. P. *Chem. Phys. Lett.* **2000**, *323*, 312.
- (9) Bigelow, R. W.; Freund, H. J.; Dick, B. *Theor. Chim. Acta* **1983**, *63*, 177.
- (10) Gordon, M. S.; Freitag, M. A.; Bandyopadhyay, P.; Jensen, J. H.; Kairys, V.; Stevens, W. J. *J. Phys. Chem. A* **2001**, *105*, 293.
- (11) Gordon, M. S.; Slipchenko, L. V.; Li, H.; Jensen, J. H. *Annu. Rep. Comput. Chem.* **2007**, *3*, 177.
- (12) Slipchenko, L. V.; Gordon, M. S. *J. Comput. Chem.* **2007**, *28*, 276.
- (13) Smith, T.; Slipchenko, L. V.; Gordon, M. S. *J. Phys. Chem. A* **2008**, *112*, 5286.
- (14) Slipchenko, L. V.; Gordon, M. S. *J. Phys. Chem. A* **2009**, *113*, 2092.
- (15) Yoo, S.; Zahariev, F.; Sok, S.; Gordon, M. S. *J. Chem. Phys.* **2008**, *129*, 144112.
- (16) Arora, P.; Slipchenko, L. V.; Webb, S. P.; Defusco, A.; Gordon, M. S. *J. Phys. Chem. A* **2010**, *114*, 6742.
- (17) Slipchenko, L. V. *J. Phys. Chem. A* **2010**, *114*, 8824.
- (18) Head-Gordon, M.; Maurice, D.; Oumi, M. *Chem. Phys. Lett.* **1995**, *246*, 114.
- (19) Head-Gordon, M.; Rico, R. J.; Oumi, M.; Lee, T. J. *Chem. Phys. Lett.* **1994**, *219*, 21.
- (20) Koch, H.; Jensen, H. J. A.; Jorgensen, P.; Helgaker, T. *J. Chem. Phys.* **1990**, *93*, 3345.
- (21) Stanton, J. F.; Bartlett, R. J. *J. Chem. Phys.* **1993**, *98*, 7029.
- (22) Sekino, H.; Bartlett, R. J. *Int. J. Quantum Chem.* **1984**, *18*, 255.
- (23) Adamovic, I.; Freitag, M. A.; Gordon, M. S. *J. Chem. Phys.* **2003**, *118*, 6725.
- (24) Day, P. N.; Jensen, J. H.; Gordon, M. S.; Webb, S. P.; Stevens, W. J.; Krauss, M.; Garmer, D.; Basch, H.; Cohen, D. *J. Chem. Phys.* **1996**, *105*, 1968.
- (25) Gordon, M. S.; Mullin, J. M.; Pruitt, S. R.; Roskop, L. B.; Slipchenko, L. V.; Boatz, J. A. *J. Phys. Chem. B* **2009**, *113*, 9646.
- (26) Ghosh, D.; Kosenkov, D.; Vanovschi, V.; Williams, C.; Herbert, J. M.; Schmidt, M. W.; Gordon, M. S.; Slipchenko, L. V.; Krylov, A. I. *J. Phys. Chem. A* **2010**, *114*, 12739.
- (27) Stone, A. J. *Chem. Phys. Lett.* **1981**, *83*, 233.
- (28) Stone, A. J. *The Theory of Intermolecular Forces*; Oxford University Press: Oxford, U.K., 1996.
- (29) Freitag, M. A.; Gordon, M. S.; Jensen, J. H.; Stevens, W. J. *J. Chem. Phys.* **2000**, *112*, 7300.
- (30) Slipchenko, L. V.; Gordon, M. S. *Mol. Phys.* **2009**, *107*, 999.
- (31) Kairys, V.; Jensen, J. H. *Chem. Phys. Lett.* **1999**, *315*, 140.
- (32) Li, H.; Netzloff, H. M.; Gordon, M. S. *J. Chem. Phys.* **2006**, *125*, 194103.
- (33) Adamovic, I.; Gordon, M. S. *Mol. Phys.* **2005**, *103*, 379.
- (34) Amos, R. D.; Handy, N. C.; Knowles, P. J.; Rice, J. E.; Stone, A. J. *J. Phys. Chem.* **1985**, *89*, 2186.
- (35) Tang, K. T.; Toennies, J. P. *J. Chem. Phys.* **1984**, *80*, 3726.
- (36) Jensen, J. H. *J. Chem. Phys.* **2001**, *114*, 8775.
- (37) Jensen, J. H.; Gordon, M. S. *Mol. Phys.* **1996**, *89*, 1313.
- (38) Jensen, J. H.; Gordon, M. S. *J. Chem. Phys.* **1998**, *108*, 4772.
- (39) Hehre, W. J.; Ditchfield, R.; Pople, J. A. *J. Chem. Phys.* **1972**, *56*, 2257.
- (40) Head-Gordon, M.; Oumi, M.; Maurice, D. *Mol. Phys.* **1999**, *96*, 593.
- (41) Thompson, M. A.; Schenter, G. K. *J. Phys. Chem.* **1995**, *99*, 6374.
- (42) Gordon, M. S.; Schmidt, M. W. In *Theory and Applications of Computational Chemistry*; Dykstra, C. E., Frenking, G., Kim, K. S., Scuseria, G. E., Eds.; Elsevier: Amsterdam, 2005; Chapter 41.
- (43) Schmidt, M. W.; Baldrige, K. K.; Boatz, J. A.; Elbert, S. T.; Gordon, M. S.; Jensen, J. H.; Koseki, S.; Matsunaga, N.; Nguyen, K. A.; Su, S. J.; Windus, T. L.; Dupuis, M.; Montgomery, J. A. *J. Comput. Chem.* **1993**, *14*, 1347.
- (44) Shao, Y.; Molnar, L. F.; Jung, Y.; Kussmann, J.; Ochsenfeld, C.; Brown, S. T.; Gilbert, A. T. B.; Slipchenko, L. V.; Levchenko, S. V.; O'Neill, D. P.; DiStasio, R. A.; Lochan, R. C.; Wang, T.; Beran, G. J. O.; Besley, N. A.; Herbert, J. M.; Lin, C. Y.; Van Voorhis, T.; Chien, S. H.;

Sodt, A.; Steele, R. P.; Rassolov, V. A.; Maslen, P. E.; Korambath, P. P.; Adamson, R. D.; Austin, B.; Baker, J.; Byrd, E. F. C.; Dachsel, H.; Doerksen, R. J.; Dreuw, A.; Dunietz, B. D.; Dutoi, A. D.; Furlani, T. R.; Gwaltney, S. R.; Heyden, A.; Hirata, S.; Hsu, C. P.; Kedziora, G.; Khaliulin, R. Z.; Klunzinger, P.; Lee, A. M.; Lee, M. S.; Liang, W.; Lotan, I.; Nair, N.; Peters, B.; Proynov, E. I.; Pieniazek, P. A.; Rhee, Y. M.; Ritchie, J.; Rosta, E.; Sherrill, C. D.; Simmonett, A. C.; Subotnik, J. E.; Woodcock, H. L.; Zhang, W.; Bell, A. T.; Chakraborty, A. K.; Chipman, D. M.; Keil,

F. J.; Warshel, A.; Hehre, W. J.; Schaefer, H. F.; Kong, J.; Krylov, A. I.; Gill, P. M. W.; Head-Gordon, M. *Phys. Chem. Chem. Phys.* **2006**, 8, 3172.

(45) Salem, L.; Rowland, C. *Angew. Chem., Int. Ed.* **1972**, 11, 92.

(46) El-Sayed, M. A. *J. Chem. Phys.* **1963**, 38, 2834.

(47) El-Sayed, M. A. *Acc. Chem. Res.* **1968**, 1, 8.

JP110026C